New adaptive optics Tomographic Pupil Image reconstructor based on convolutional neural networks

C. González Gutiérrez[a], J. J. Fernández Valdivia[b], S. L. Suárez Gómez*[a], J. M. Rodríguez Ramos[b], L. F. Rodríguez Ramos[c], F. J. de Cos Juez [a]

[a]Department of Exploitation and Exploration of Mines, University of Oviedo, Oviedo, Spain; [b] Wooptix S.L., San Cristobal de La Laguna, Spain; [c] Instituto de Astrofísica de Canarias, San Cristobal de La Laguna, Spain.

ABSTRACT

Astronomical images taken from large ground-based telescopes requires techniques as Adaptive Optics in order to improve their spatial resolution. In this work are presented computational results from a modified curvature sensor, the Tomographic Pupil Image Wavefront Sensor (TPI-WFS), which measures the turbulence of the atmosphere, expressed in terms of an expansion over Zernike polynomials. Convolutional Neural Networks (CNN) are presented as an alternative to the TPI-WFS reconstruction. This technique is a machine learning model of the family of Artificial Neural Networks (ANN), which are widely known for its performance as modeling and prediction technique in complex systems. Results obtained from the reconstruction of the networks are compared with the TPI-WFS reconstruction by estimating errors and optical measurements (Root Mean Square error, Mean Structural Similarity and Strehl ratio).

In general, CNN trained as reconstructor showed slightly better performance than the conventional reconstruction in TPI-WFS for most of the turbulent profiles, but it made significant improvements for higher turbulent profiles that have the lowest r0 values.

Keywords: Adaptive Optics, TPI-WFS, Convolutional Neural Networks.

1. INTRODUCTION

Adaptive Optics (AO) is the main technique to improve the spatial resolution of large ground-based telescopes [1]. It has turned to provide excellent results on offering diffraction limited images in the near infrared, due to the minor effects of turbulence in this range.

In the optical bands AO systems on duty today are able to achieve high success in correcting the incoming wavefront errors at high degrees by using Shack-Hartmann (SH) sensors, but they require very bright, and hence scarce, reference stars or a laser non-natural star [2].

In a previous work, we have proposed a modified curvature sensor, the Tomographic Pupil Image Wavefront Sensor (TPI-WFS), to be used instead of a classical SH sensor [3]. This new sensor has been demonstrated that it can successfully measure the turbulence of the atmosphere. Furthermore, it presents also some advantages. For example, it has better resolution than a SH sensor, it can work with low light illumination regime and it is stable when changes in the optical parameters are introduced.

Artificial Neural Networks (ANN) are a type of machine learning technique, which are known for its capacity of modeling complex systems [4–8]. In the field of AO, techniques as ANNs have been proven to be very useful with the use of SH sensors as, for example, the Complex Atmospheric Reconstructor based on Machine lEarNing (CARMEN) [9]. This reconstructor algorithm use information from the SH sensor to estimate the atmospheric turbulence [10]. The improvements and characteristics of this artificial intelligence approach have been widely studied for the adaptive optics reconstruction [11,12]. CNN have been widely used in image recognition, language processing, etc., achieving great success [13].

*suarezsergio@uniovi.es

CNNs are a machine learning technique of the family of ANNs [14–16], which are widely known for its usage as a modeling and prediction technique in complex systems [16,17] as well as its performance in AO [18,19]. One of the best advantages that CNN provides is that it allows full images as inputs, since the process will involve the extraction of the main characteristics in each convolutional layer into feature maps that will be, later, reduced in size.

In this work a comparison between a real time TPI-WFS restoration and a CNN reconstruction was made by computational simulations implemented on a Graphics Processor Unit (GPU).

The paper will enclose the following contents. In section 2, an explanation about the techniques is presented. These techniques were used in this work for sensing and turbulent image reconstruction. Also, the setup of the network and its correspondent training is detailed in this section. In section 3, the results of the performance of both methods of reconstruction is shown, considering optical and absolute error measurements. These results are later compared in section 4, where the discussion and explanation of the behavior of the models and its results is introduced. Finally, in section 5 the conclusions of the work are presented, along with some insights on the possible future lines that this work leads to.

2. METHODS AND TECHNIQUES

2.1 TPI-WFS

The TPI–WFS uses a technique for deriving the wavefront aberration from two intensity measurements (I_1 and I_2) using the first derivative of the wavefront, rather than contrast proportional to the Laplacian of the phase (as in curvature sensors). The photon shift measurements in different projections can be expressed as an expansion over Zernike polynomials using a least squares fit. This way of expressing the results, either as a set of coefficients or as surface, facilitates the wavefront compensation by using a deformable mirror, as it is shown in Figure 1.

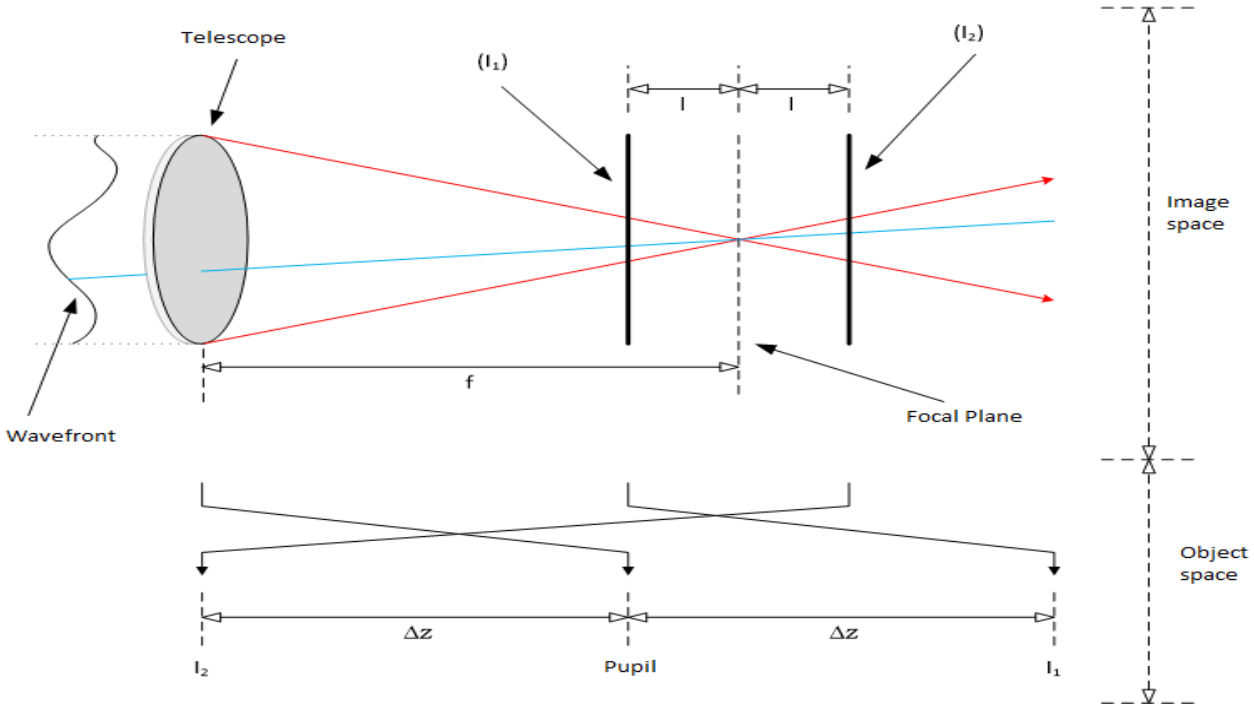

Figure 1. Conceptual diagram of a curvature sensor. Design from [2].

2.2 Convolutional Neural Networks

Adapting CNNs to a given training data implies the usage of filters in each convolutional layer, which are adjusted in the training process to extract the most relevant features from the data to be modeled. This process can be repeated through

several layers until reaching a fully connected Multi-Layer Perceptron (MLP) that provides the output [20]. The MLP has, as inputs, the features selected with the convolutional layers.

Training process also involves the adjustment of the weights in the connections between the neurons of adjacent layers of the MLP, as well as the weights of the filters from the convolutional layers.

In Figure 2 is shown how the usual topology of a CNN is represented. The image is given as an input to the network, which is followed by sets of convolutional and subsampling layers. Each convolutional layer extracts a defined number of feature maps, which will have its size reduced after being processed by the sub-sampling layer. This process is repeated the desired amount of times until reaching the MLP.

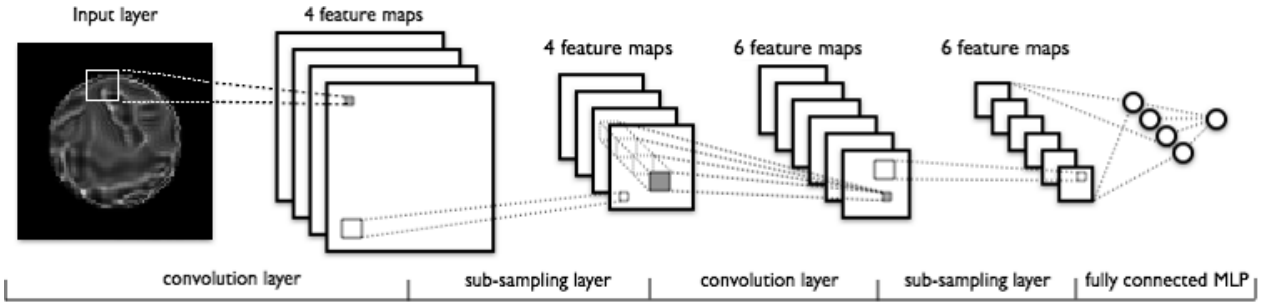

Figure 2. Example of the topology and implementation of a convolutional neural network. After the sequences of convolution and sub-sampling layers, the output feature maps are connected to a multi-layer perceptron.

2.3 Simulations.

Model used for the reconstruction was a CNN which was trained with phases of 25 Zernike modes, from turbulence simulations with r0 ranging from 5 cm to 20 cm, and wavelength of 590 nm. As the original TPI-WFS was designed for an AO system that corrected the first 25 Zernike modes, the simulations were performed to represent a telescope with a deformable mirror that also allows correction of the first 25 Zernike modes. The recovered phases obtained by both reconstructors, TPI-WFS and CNN reconstruction, were compared with the reference phase, corresponding to the original simulated phase. The comparison was made between the recovered phases using 25 Zernike modes, since the deformable mirror that were in the TPI-WFS has this resolution as limitation, and the reference phase which contains 153 Zernike modes.

Specifically, the chosen network used for training 1500000 images of 56 pixels of side as inputs. These images had 2 channels, corresponding with the I_1 and I_2 presented in Figure 1. The network had 4 convolutional layers, each of them with four filters of size 3x3, shifting 1 pixel horizontally in each step, and then, 1 vertically. In order to do this along all the image, 1 zero was padded outside of the edges of each image. After each convolutional layer, a rectified linear unit is applied [21]. Also, after the second convolutional layer, Max-Pooling, a sample-based discretization process [22,23] is applied in sections of 4x4 , and after the fourth in sections of 7x7.

The number of images increased in 4 times for each convolutional layer (due to the 4 filters in each layer), leading to 512 images of size 2x2 at the end of the convolutions. This represents 2048 values which are the input values of the neurons that conformed the fully connected MLP. Each of these input neurons were paired all the 2048 neurons set to conform the hidden layer. At last, these were connected with the 25 output neurons, which corresponds with the 25 desired estimations of the Zernike coefficients. Also, another set of 100000 different images was used for testing in the training process.

3. RESULTS

3.1 Comparison and results

Results obtained from the reconstruction of the CNN can be compared with the TPI-WFS reconstruction by means of optical measurements, such as Root Mean Square (RMS) error, Mean Structural Similarity (MSSIM) and Strehl ratio.

The RMS error is calculated with each of the recovered phases compared with a reference phase. As it can be seen in Figure 3, the error decreases in the less turbulent scenarios for both methods, as the value of r0 increases. For the most turbulent scenarios the CNN shows better results for the reconstruction.

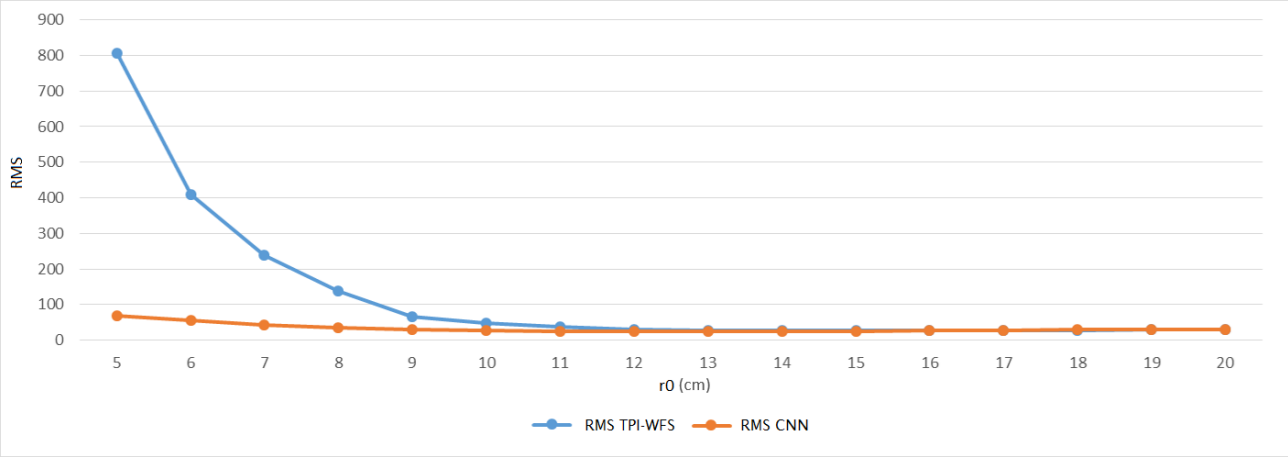

Figure 3. Root Mean Square error of the difference between a recovered phase image and the reference one with the Convolutional Neural Network reconstruction and the Tomographic Pupil Image Wavefront Sensor reconstruction.

MSSIM is shown in Figure 4, measuring the image quality of the reconstructions obtained from both methods. Best results are obtained by the CNN with values from 5 to 12 cm, from this value, results of both technique were very similar. As happened with the RMS, the results of the CNN in the most turbulent scenarios improves the ones of the reconstructor in TPI-WFS. Overall, both methods work well in terms of image quality.

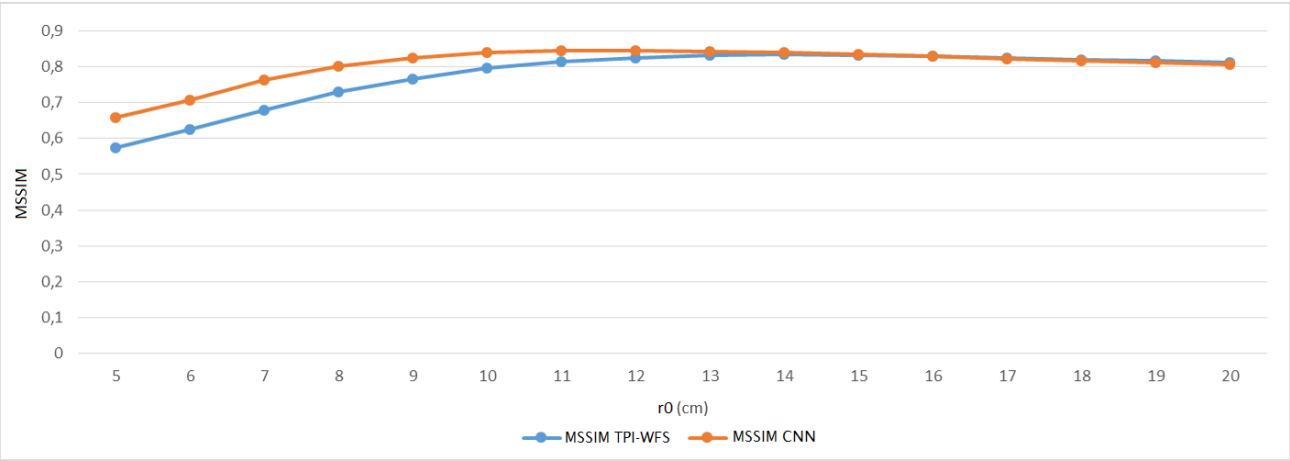

Figure 4. Mean Structural Similarity index for measuring image quality between a recovered phase image and the reference one with the Convolutional Neural Network reconstruction and the Tomographic Pupil Image Wavefront Sensor reconstruction.

Results of the Strehl ratio are shown in Figure 5. Both methods showed improvements as the value of r0 raises and consequently in less turbulent profiles. The CNN shows better performance than the TPI-WFS reconstruction in all the cases.

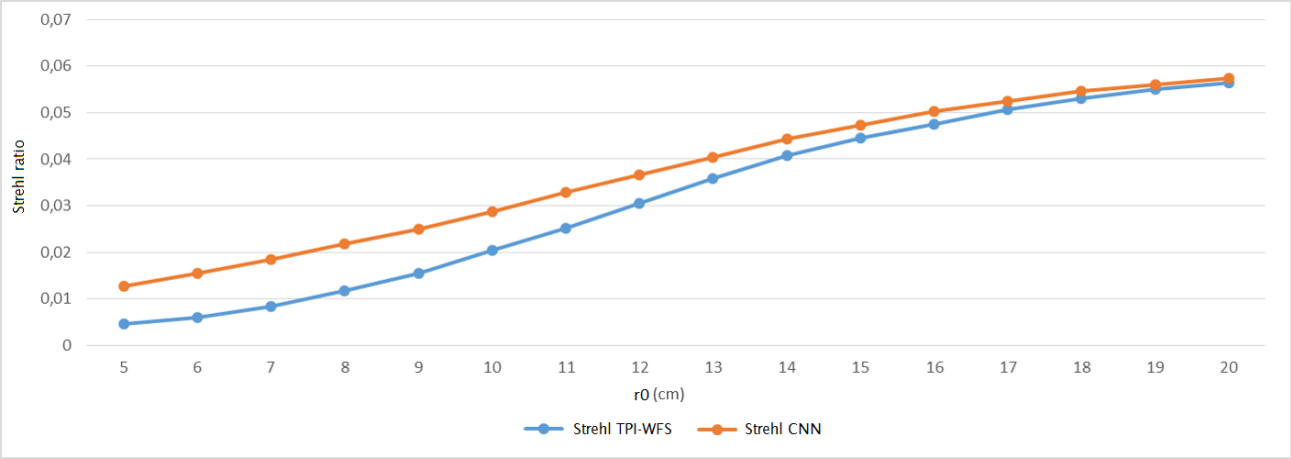

Figure 5. Strehl ratio of the difference between a recovered phase image and the reference one, measuring similarity with the Convolutional Neural Network reconstruction and the Tomographic Pupil Image Wavefront Sensor reconstruction.

The images, as an example of the results from the reconstruction with both systems, can be shown in Figure 6. These images support the results presented above, with both reconstructors performing a notable approach.

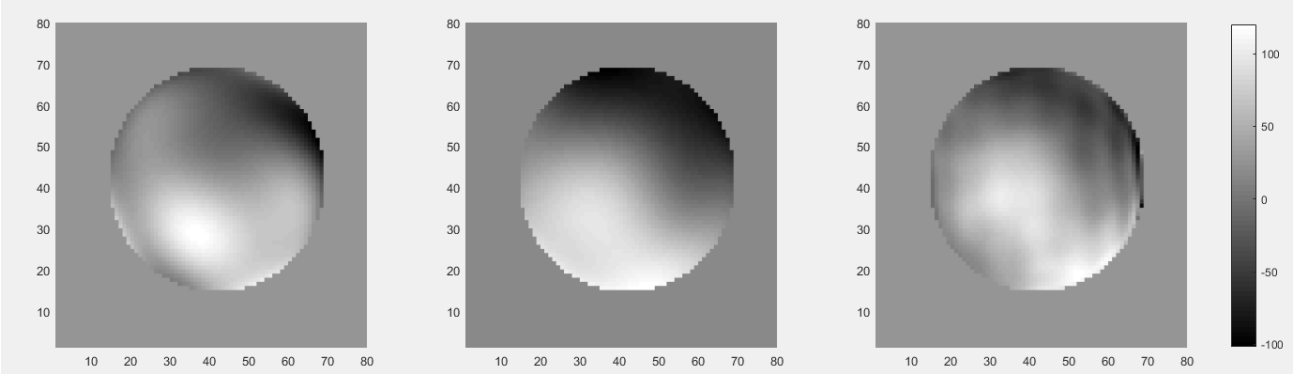

Figure 6. From left to right, Tomographic Pupil Image Wavefront Sensor recovered phase, Convolutional Neural Network recovered phase and Reference phase with 153 Zernikes. All are 80x80 pixels images representing the pupil of 56 pixels as diameter.

4. DISCUSSION

In general, the CNN reconstruction showed slightly better performance than the TPI-WFS reconstruction for the slightest turbulent scenarios, and made notable improvements for higher turbulent profiles that have the lowest r0 values, as can be seen in the Figures 3, 4 and 5.

On the other hand, the CNN needed to be trained again every time that a parameter of the simulated optical arrangement was modified. Nevertheless, further studies are warranted including noise and low light illumination.

The main reason for the improvements achieved by the CNN relies in the training procedure. Since computational simulations were available, which allowed to generate data with enough variability to cover all the turbulent profiles satisfactorily. In particular, the most turbulent scenarios, where the r0 reach its lowest values, has the same importance in the training as the rest of profiles. Consequently, the notable results in these cases are reasonable, concretely when considering direct measurements of the error, such as in the RMS case, where the differences are more noticeable.

Values obtained for the Strehl ratio are lower than the usuals, due to the simulated system corrects the first 25 Zernike modes of the input phase, for the posterior usage of the Lucky Imaging technique. This implies a limitation on the obtainable maximum Strehl ratio. In the cases where the correction is performed only with the deformable mirror, the advantages of machine learning were already proven, as in the case of CARMEN [9]. In the case of TPI-WFS, when used with Lucky Imaging, promising results can be obtained, even with images of higher resolution, but the utilization of machine learning was not tested yet. However, a CNN can also be trained to obtain a higher number of Zernikes in systems with corrections based on the characteristics of a deformable mirror.

5. CONCLUSIONS

The artificial network approach to the AO image reconstruction correspondent to TPI-WFS data was adequate. The usage of CNN as technique gave notable results thanks to the advantage of allowing the usage of images as inputs and the capability of extracting its main features.

Performance of both methods for phase reconstruction has been compared. In this study performed with computational simulations, the CNN approach was revealed as a promising method. Both methods showed notable result in the majority of turbulent profiles, however, the CNN improved the TPI-WFS reconstruction, giving better results, in average, for the strongest turbulence cases.

Usage of other techniques of artificial intelligence suppose the possibility of increasing the performance of the reconstruction. Methods as recurrent real time learning, suggest that more information from the data can be learned in the training process on a neural network.

REFERENCES

1. Roddier, F. *Adaptive optics in astronomy*; Cambridge university press, 1999.

2. Roddier, C.; Roddier, F. Wave-front reconstruction from defocused images and the testing of ground-based optical telescopes. *JOSA A* **1993**, *10*, 2277–2287.

3. Colodro-Conde, C.; Velasco, S.; Fernández-Valdivia, J. J.; López, R.; Oscoz, A.; Rebolo, R.; Femenía, B.; King, D. L.; Labadie, L.; Mackay, C.; others Laboratory and telescope demonstration of the TP3-WFS for the adaptive optics segment of AOLI. *Mon. Not. R. Astron. Soc.* **2017**, *467*, 2855–2868.

4. Fernández, J. R. A.; Muñiz, C. D.; Nieto, P. J. G.; de Cos Juez, F. J.; Lasheras, F. S.; Roqueñí, M. N. Forecasting the cyanotoxins presence in fresh waters: A new model based on genetic algorithms combined with the MARS technique. *Ecol. Eng.* **2013**, *53*, 68–78.

5. De Andrés, J.; Sánchez-Lasheras, F.; Lorca, P.; JUEZ, F. J. de Cos. A hybrid device of Self Organizing Maps (SOM) and Multivariate Adaptive Regression Splines (MARS) for the forecasting of firms' bankruptcy. *Account. Manag. Inf. Syst.* **2011**, *10*, 351.

6. Turrado, C. C.; López, M. del C. M.; Lasheras, F. S.; Gómez, B. A. R.; Rollé, J. L. C.; Juez, F. J. de C. Missing data imputation of solar radiation data under different atmospheric conditions. *Sensors* **2014**, *14*, 20382–20399.

7. de Cos Juez, F. J.; Lasheras, F. S.; Nieto, P. J. G.; Álvarez-Arenal, A. Non-linear numerical analysis of a double-threaded titanium alloy dental implant by FEM. *Appl. Math. Comput.* **2008**, *206*, 952–967.

8. Casteleiro-Roca, J.-L.; Calvo-Rolle, J. L.; Méndez Pérez, J. A.; Roqueñí Gutiérrez, N.; de Cos Juez, F. J. Hybrid Intelligent System to Perform Fault Detection on BIS Sensor During Surgeries. *Sensors* **2017**, *17*, 179.

9. Osborn, J.; De Cos Juez, F. J.; Guzman, D.; Butterley, T.; Myers, R.; Guesalaga, A.; Laine, J. Using artificial neural networks for open-loop tomography. *Opt. Express* **2012**, *20*, 2420.

10. Osborn, J.; Guzman, D.; Juez, F. J. D. C.; Basden, A. G.; Morris, T. J.; Gendron, E.; Butterley, T.; Myers, R. M.; Guesalaga, A.; Lasheras, F. S.; Victoria, M. G.; Rodríguez, M. L. S.; Gratadour, D.; Rousset, G. Open-loop tomography with artificial neural networks on CANARY: On-sky results. *Mon. Not. R. Astron. Soc.* **2014**, *441*, 2508–2514.

11. Suárez Gómez, S. L.; Gutiérrez, C. G.; Rodríguez, J. D. S.; Rodríguez, M. L. S.; Lasheras, F. S.; de Cos Juez, F. J. Analysing the Performance of a Tomographic Reconstructor with Different Neural Networks Frameworks. In *International Conference on Intelligent Systems Design and Applications*; 2016; pp. 1051–1060.

12. González-Gutiérrez, C.; Santos-Rodríguez, J. D.; Díaz, R. Á. F.; Rolle, J. L. C.; Gutiérrez, N. R.; de Cos Juez, F. J. Using GPUs to Speed up a Tomographic Reconstructor Based on Machine Learning. In *International Conference on EUropean Transnational Education*; 2016; pp. 279–289.

13. Krizhevsky, A.; Sutskever, I.; Hinton, G. E. Imagenet classification with deep convolutional neural networks. In *Advances in neural information processing systems*; 2012; pp. 1097–1105.

14. Simard, P. Y.; Steinkraus, D.; Platt, J. C.; others Best Practices for Convolutional Neural Networks Applied to Visual Document Analysis. In *ICDAR*; 2003; Vol. 3, pp. 958–962.

15. Blanco-Rodríguez, P.; Fernández-Serantes, L. A.; Otero-Pazos, A.; Calvo-Rolle, J. L.; de Cos Juez, F. J. Radon Mitigation Approach in a Laboratory Measurement Room. *Sensors* **2017**, *17*, 1090.

16. Suárez Gómez, S. L.; Santos Rodríguez, J. D.; Iglesias Rodríguez, F. J.; de Cos Juez, F. J. Analysis of the Temporal Structure Evolution of Physical Systems with the Self-Organising Tree Algorithm (SOTA): Application for Validating Neural Network Systems on Adaptive Optics Data before On-Sky Implementation. *Entropy* **2017**, *19*, 103.

17. González-Gutiérrez, C.; Santos, J. D.; Martínez-Zarzuela, M.; Basden, A. G.; Osborn, J.; Díaz-Pernas, F. J.; De Cos Juez, F. J. Comparative Study of Neural Network Frameworks for the Next Generation of Adaptive Optics Systems. *Sensors* **2017**, *17*, 1263.

18. Osborn, J.; Juez, F. J. D. C.; Guzman, D.; Butterley, T.; Myers, R.; Guesalaga, A.; Laine, J. Using artificial neural networks for open-loop tomography. *Opt. Express* **2012**, *20*, 2420–2434.

19. de Cos Juez, F. J.; Lasheras, F. S.; Roqueñí, N.; Osborn, J. An ANN-based smart tomographic reconstructor in a dynamic environment. *Sensors (Switzerland)* **2012**, *12*, 8895–8911.

20. Hornik, K.; Stinchcombe, M.; White, H. Multilayer feedforward networks are universal approximators. *Neural networks* **1989**, *2*, 359–366.

21. Nair, V.; Hinton, G. E. Rectified linear units improve restricted boltzmann machines. In *Proceedings of the 27th international conference on machine learning (ICML-10)*; 2010; pp. 807–814.

22. Giusti, A.; Ciresan, D. C.; Masci, J.; Gambardella, L. M.; Schmidhuber, J. Fast image scanning with deep max-pooling convolutional neural networks. In *Image Processing (ICIP), 2013 20th IEEE International Conference on*; 2013; pp. 4034–4038.

23. Nagi, J.; Ducatelle, F.; Di Caro, G. A.; Cirçsan, D.; Meier, U.; Giusti, A.; Nagi, F.; Schmidhuber, J.; Gambardella, L. M. Max-pooling convolutional neural networks for vision-based hand gesture recognition. In *Signal and Image Processing Applications (ICSIPA), 2011 IEEE International Conference on*; 2011; pp. 342–347.